

LIGHTNING NO_x AND TROPOSPHERIC OZONE FORMATION IN THE NASA GISS GLOBAL CARBON MODEL

Amanda E. Hopkins, Florida State University, Tallahassee, FL (ahopkins@met.fsu.edu)
Mentor: Dr. Drew Shindell, NASA Goddard Institute for Space Studies

Abstract. *Tropospheric ozone formation from NO_x produced by lightning, and its radiative forcing are studied using the NASA Goddard Institute for Space Studies (GISS) global climate model (GCM) with interactive chemistry. The effect on tropospheric ozone due to lightning is presented for present day conditions. Lightning NO_x has the most influence on ozone formation in the upper troposphere for the austral summer (December, January, and February) and is slightly lower for the boreal summer (June, July, and August). The influence of lightning NO_x on the formation of ozone in the model can be seen throughout the troposphere. The global average total radiative forcing at the tropopause due to ozone formed by lightning NO_x is +0.1W/m² in June, July, and August, and +0.12W/m² in December, January, and February. Locally, the radiative forcing is as high as +0.24W/m² in the mid-latitudes, and as high as +0.3W/m² in the northern high latitudes in June, July and August. In December, January, and February, locally, net radiative forcing is the highest from approximately 20S to 50S, and ranges from +0.2 to almost +0.4W/m². The possible future changes in lightning, in a doubled CO₂ simulation, are also examined and presented. Lightning increases 30% per degree of warming in June, July, and August, and 20% in December, January, and February. This increase in lightning presumably providing an increase in NO_x, and therefore tropospheric ozone is expected to increase. The model results presented here suggest the sensitivity of ozone to lightning is greatest in tropical and subtropical regions particularly over the Atlantic Ocean in the upper troposphere. The radiative forcing due to tropospheric ozone from lightning NO_x is small, but not negligible, and could imply the possibility of a positive climate feedback mechanism.*

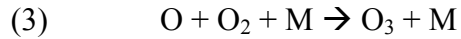
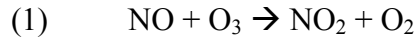
INTRODUCTION

Tropospheric ozone

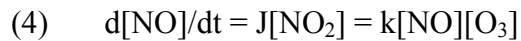
Tropospheric ozone plays an important role in both changes in global climate and the oxidation capacity of the atmosphere. Roughly 10% of the Earth's ozone is found in the troposphere, where it plays a key role in providing oxidizing radicals, OH•, that cleanse the lower atmosphere of pollutants, such as carbon monoxide (CO), and sulfur dioxide (SO₂). However, high concentrations of ozone at ground level can be toxic to plants, and an irritant to humans, and high concentrations of ozone in the upper troposphere can affect atmospheric radiative properties.

The formation of tropospheric ozone is highly nonlinear, meaning that the rates of accumulation are not proportional to the rates of precursor emissions. Formation depends on numerous factors such as, precursor emissions, horizontal and vertical transport, clouds and aerosols, etc. Prior to the 1940s, it was thought that the source of tropospheric ozone was solely stratospheric injections. By the mid-1940s, it became obvious that ozone could be produced in the troposphere. After damage to vegetation occurred in the Los Angeles area, Haagen-Smit (1952) showed that the damaged was due to ozone. The “photochemical smog” has ozone concentrations too high to be from stratospheric origin, and the reactions mechanisms were identified. Ozone formation is possible by photodissociation of NO₂,

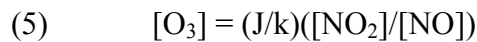
into NO and O, by solar radiation of wavelengths between about 300nm and 400nm. Atomic oxygen (O) then combines with molecular oxygen (O₂) to form ozone (O₃).



The reactions discussed above establish the photostationary state, where ozone concentration depends on the ratio of NO₂ to NO rather than their individual concentrations. In a steady state situation, the rates of change of NO concentration should be equal:



where, J and k are the photodissociation rate and reaction rate constant of the two reactions, respectively. Solving equation (1) shows that ozone concentration depends on the ratio of NO₂ to NO:

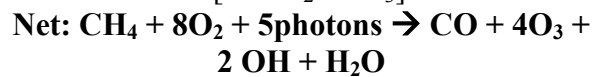
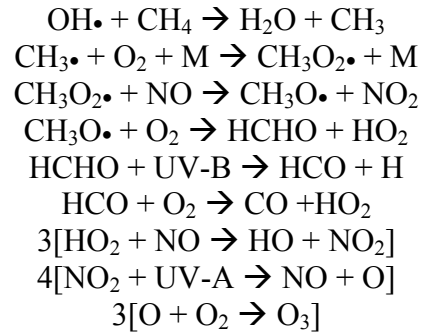


Therefore, in order to get an accumulation of ozone other reactions are needed to oxidize NO to NO₂ without consuming O₃.

In the 1970s, it was proposed that in-situ production of ozone was taking place on global scales (Crutzen, 1973, 1974; Chameides and Walker, 1973). Levy (1971) proposed that ozone photolysis at wavelengths shorter than 310nm leads to the production of hydroxyl (OH), which plays a significant role in the removal of many gases produced naturally and anthropogenically. Crutzen (1973, 1974) postulated that ozone could both be produced and destroyed by the methane and carbon monoxide oxidation cycles, depending on nitric oxide (NO) concentrations.

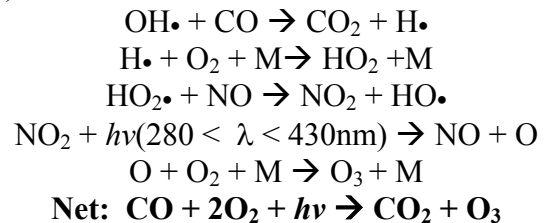
Oxidation of methane yields CO, O₃, and OH as its principal products via oxidation chains such as the following:

(6)



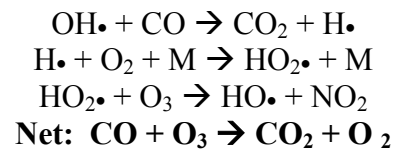
Carbon monoxide cycles can either proceed via:

(7)



or by:

(8)



The availability of NO_x is crucial to reactions (7) and (8). In the case where NO_x is high, reaction (7) will occur, whose rate coefficient is 4,000 times faster than the rate coefficient of reaction (8), which occurs when NO_x is low. Nitrogen dioxide generated by the oxidation of CH₄ (reactions 6) and CO, can then produce O₃ by way of photodissociation of NO₂. Through these processes the ratio between NO₂ and NO can rise without sacrificing a lot of O₃, and therefore, the

concentration of ozone rises. Tropospheric ozone formation is complex and depends on many factors: The availability of NO and NO₂ being two of the most important. In order to better understand tropospheric ozone's radiative properties the effect of NO_x emissions on this secondary greenhouse gas must be evaluated.

Nitrogen Oxides

Global NO_x (NO+NO₂) has various sources, including fossil fuel combustion, biomass burning, aircraft emission, microbial processes in the soil, and lightning (Tie et al. 2002, Grewe et al., 2001, etc....). The sources and sinks in the GISS chemistry model have been compiled from the Global Emission Inventory Activity (GEIA) data set (Benkovitz et al., 1996; Olivier et al., 1996). This data set consists of annual emissions from fossil fuel burning (20.9 Tg N yr⁻¹), monthly emissions from biomass burning (5.8 Tg N yr⁻¹), soils (5.8 Tg N yr⁻¹), and aircraft (0.6 Tg N yr⁻¹). Lightning, which is calculated internally in the model, contributes about 16% (6.5 Tg N yr⁻¹) to the NO_x global budget, while fossil fuel burning and biomass burning contribute close to 70% of the NO_x budget.

Measured concentrations of NO_x have substantial spatial and temporal variability. This is due to the fact that the local chemical lifetime of NO_x is less than 1 day in the polluted boundary layer, and 5 to 10 days in the upper troposphere. The effect of lightning on the NO_x budget is important to NO_x in the upper troposphere, where the lifetime is longer. Many studies have looked at lightning produced NO_x (Price et al., 1997; Pickering et al., 1998). The next section describes lightning processes.

Lightning

Lightning is associated with the occurrence of deep convection, and the presence of ice and supercooled water

droplets, but the specific mechanism attributed to cloud electrification is still unsettled. In a typical (positive dipole) thunderstorm, a net negative charge is observed near the cloud base, and a net positive charge is observed in the upper region of the cloud (Price et al., 1997). There are three types of lightning discharge; cloud-to-ground (CG), intracloud (IC), and intercloud (cloud to cloud).

There are cloud-to-ground flashes that bring negative charges to the earth, and there are CG flashes that bring positive charges. Most charges are negative due to the proximity of the negatively charged region in the cloud (Price et al., 1997). A process called preliminary breakdown begins within a cloud lasting for tens of milliseconds, and initiates an intermittent, highly branched discharge called a stepped leader. As the downward propagating leader gets close to the ground, an upward propagating discharge (called a streamer), is initiated from the ground. When they meet, the return stroke, a large current pulse, starts at the ground and propagates back up the leader channel to the cloud. Sometimes additional charge is available and a dart stroke propagates back down the previous return stroke channel, which initiates a subsequent stroke.

Most lightning occurs within the clouds during a thunderstorm. The electrification of a cloud happens in the mixed-phase region of the cloud, resulting from interactions between ice particles and supercooled droplets. It has been observed that clouds with larger volumes above the freezing level have more IC flashes than CG flashes, which explains why the IC/CG ratio is larger in the tropics than midlatitudes (Pickering et al., 1998).

Nitric oxide is produced in the hot lightning channel by way of the Zel'dovich mechanism, which considers the break up of N₂ and O₂ molecules (Zel'dovich and Raizer, 1966). This mechanism takes place due to the high temperatures and pressures initiated by

the lightning stroke. NO is produced as the shock front propagates outward through a volume of air. As the channel cools from the outside inward, the amount of NO is determined by the cooling rate. NO_x is produced primarily during the high-energy return stroke phase of the flash, and is 75-95% NO (Price et al., 1997). The leaders may also contribute to NO_x production, however, their radius is an order of a magnitude smaller than the radius of a return stroke, and therefore they produce much less NO_x. According to Price et al. (1997) CG flashes produce 6.7×10^{26} molecules NO per flash, where IC flashes produce 6.7×10^{25} molecules NO per flash. The IPCC report (2001) states that lightning produced NO_x is still quite uncertain and is in the range of 2-20 Tg N yr⁻¹, while other results have suggested 7.0 (Exhalt 1999), 3-13 (Holland et al., 1999), 3-5 (Penner et al., 1999), and 5.0 Tg N yr⁻¹ (Lee et al., 1997).

METHODS

Chemical Transport Model

The tropospheric chemistry model used at Goddard Institute for Space Studies (GISS) within the general circulation model (GCM) includes the basic HO_x-NO_x-O_x-CO-CH₄ chemistry as well as peroxyacetylnitrates (PANs) and non-methane hydrocarbons (Shindell et al., 2003). This model uses the “chemical family” approach, which means that radical species in particular families are grouped together, and a family is transported as one species. This approach allows calculations requiring the transport of only 16 species in the GCM, which are described in Shindell et al. (2003). Computation time is further cut as reactions between family members are assumed to be rapid enough to maintain steady state. The “lumped family” approach is used for hydrocarbons and PANs. Chemical reactions involving these gases are based on the similarity between molecular

bond structures within each family using the Carbon Bond Mechanism 4 (Gery et al., 1989; Houweling et al., 1998). Both of the aforementioned techniques allow a larger chemical time step, which is 1 hour in these experiments. The chemical scheme includes 77 reactions as well as heterogeneous hydrolysis of N₂O₅ into HNO₃ (taking place on sulfate aerosols). Photolysis rates are calculated every 2 hours using the FAST-J scheme (Wild et al., 2000). Phase transformations are calculated based on the GCM’s internal cloud scheme. The model also includes transport within convective plumes, scavenging within and below updrafts, rainout within convective and large-scale clouds, washout below precipitation regions, evaporation of falling precipitation, and detrainment and evaporation from convective plumes. In addition to the aforementioned parameterizations, the GISS tropospheric chemistry scheme, unlike most chemical models, includes a detailed global methane cycle as well as global hydrological cycle. Chemical calculations are for the troposphere only. The stratospheric O₃, NO_x, and CH₄ have been prescribed by satellite-measured quantities and vary seasonally (Hansen et al., 1996).

Emissions are based on the Global Emissions Inventory Activity (GEIA) data sets (Benkovitz et al., 1996; Olivier et al., 1996). Total emissions for CO are 987.7 Tg yr⁻¹, of which 490.1 is from biomass burning and 497.6 from industrial activity. External NO_x emissions are from fossil fuels (20.9 Tg N yr⁻¹), soil (5.8 Tg N yr⁻¹), biomass burning (5.8 Tg N yr⁻¹), and aircraft (0.6 Tg N yr⁻¹). Approximately 6.5 Tg N yr⁻¹ is contributed by lightning (Shindell et al., 2003). Isoprene emissions are based on Wang et al., (1998), and alkenes and paraffins are from GEIA data sets. Global annual average emissions of isoprene are 200 Tg yr⁻¹, and alkenes (mainly propene) are 32.9 Tg yr⁻¹, of which 11.6 is from industry, 16.0 is from vegetation, and

5.3 is from biomass burning. Total emissions of paraffins (eg. Butane, pentane) are 87.0 Tg yr; vegetation contributes 14.0 Tg yr⁻¹, industry contributes 68.8, and biomass burning 4.2 Tg yr⁻¹. Methane emissions are based on Fung et al. (1991). The total lightning and cloud-to-ground lightning is derived by the GISS convection scheme in each grid box at each time step (Price et al., 1997). Pickering et al., 1998, describe the generation of NO_x produced by derived lightning. The flash rate is proportional to the maximum altitude reached by convective updrafts.

Climate Model

The current version of the GCM is called GISS model II' (two-prime). The GCM's boundary layer employs a finite modified Ekman layer with parameterizations for drag and mixing coefficients based on similarity theory, convection includes entraining and nonentraining plumes, max fluxes proportional to convective instability, explicit downdrafts, and a cloud liquid water scheme. The land-surface parameterization calculates transpiration, infiltration and soil water flow and runoff, which impact water vapor and latent heat release. Advection of chemical tracers as well as heat and moisture is achieved by the quadratic upstream scheme (Prather, 1986). Momentum advection used a 4th order scheme, and stratospheric-tropospheric exchange is accurately modeled using the gravity-wave drag scheme. The model used in these experiments has 4°×5° resolution in the horizontal and 23-layer vertical resolution, of which the bottom 11 are sigma levels and the top 12 are constant pressure. The physics time step is 1 hour.

RESULTS

Present day experiment

Model ozone is a result of running the GISS II' model for five years following a one

year spin up. The model's ability to produce ozone and NO_x is well documented in Shindell et al. (2003). Figure 1a-b shows climatology of seasonal averages for total model ozone (Dobson Units) for June, July, and August (JJA) and December, January, and February (DJF), respectively. Features to point out are the equatorial minimum, which is mostly constant through both seasons, and the maximum in the North Pole occurring in both seasons. Another interesting feature in the DJF plot is that the northern latitudes have much higher ozone concentrations than the southern latitudes indicating the southern hemisphere summer. Overall, JJA has slightly lower total ozone in the high latitudes and poles as compared to the DJF total ozone. Figure 2a-b shows the model's zonal averaged vertical distribution of ozone in JJA and DJF, respectively. This distribution shows clearly that 90% of ozone is located in the stratosphere, where only about 10% is found in the troposphere. In the equatorial region, the tropopause is higher, and therefore much of the ozone is found above 200hPa. At higher latitudes, where the tropopause is lower, ozone begins to increase at around 400 hPa.

Lightning NO_x

Two present day experiments were completed. One run which includes all of the model schemes called the control run, and one that has excluded the lightning scheme. Figure 3a-b shows the vertical distribution of NO_x in the control run for JJA and DJF, respectively. JJA has higher NO_x concentrations in the Northern Hemisphere with a maximum occurring between 200 and 250hPa. Two features of interest are the maximum occurring at 45N at the surface as well as 250hPa. DJF has the majority of NO_x occurring in the equatorial region of the Southern Hemisphere with the same maximums occurring at around 250 hPa. At the surface around the equatorial region there

are slightly higher NO_x values; however, the maximum at the surface is still seen at 45N.

Figure 4a-b shows the difference in NO_x between the control run and the no lightning run for JJA and DJF, respectively. This figure shows NO_x after advection and convection has occurred, meaning that it represents the portion of NO_x leftover including both sources and sinks. Figure 5a-b shows the portion of NO_x produced from lightning only, for JJA and DJF, respectively. Meaning that Figure 5 only shows the amount of NO_x from the lightning source and does not include sinks. In JJA, when lightning flashes are the greatest during northern hemisphere summer, the maximum NO_x produced by lightning occurs between 150 and 500 hPa in the Northern Hemisphere (refer to Figure 6 for global total lightning distribution). There is also a small feature at the surface showing a maximum in lightning produced NO_x . Figure 4 does not show the surface NO_x because the lifetime of NO_x at the surface is very short (<1 day). In DJF, when the lightning has the greatest occurrence in the southern subtropics during the Southern Hemisphere summer, the maximum in NO_x occurs from the equator to approximately 30S (see Figure 6 for total lightning distribution). Again, the surface NO_x in Figure 5 does not appear in Figure 4 because the chemistry at the surface reacts quickly to turn NO_x into other species such as nitric acid.

Ozone produced by lightning NO_x

Figures 7 and 8a-f show the JJA and DJF difference between the lightning (control run) and no lightning case for O_3 in ppbv for 171hPa, 218hPa, 279hPa, 370hPa, 500hPa, and 640hPa, respectively. These levels were chosen due to the impact of lightning on the NO_x concentration there (see Figure 5). In Figures 7 and 8, the blue is referring to negative values, corresponding to no impact of lightning on ozone concentrations, and the red refers to positive values, or increases in

ozone due to lightning. The hatching on these plots indicates statistical significance within a 95% confidence interval. The mid-to-high latitudes, in the plots above 370hPa, exhibit strong changes in ozone concentration between the two experiments. Some of the high and low patterns of ozone are statistically significant, however, without further research it is questionable as to whether these are simply just strong gradients in ozone due to strong temperature and potential vorticity gradients in midlatitude wave trains, or if lightning has affected this region.

In JJA, the 370hPa level has the highest global average (6.47ppbv), where in DJF, the 279hPa level has the highest global average (6.65 ppbv). A maximum occurs from 30S to 30N stretching over South America and South Africa and over the Atlantic Ocean. This maximum extends across Asia and over the Pacific Ocean. The model shows a positive effect of lightning on the ozone concentration in this area, which ranges from 8-20ppbv. These effects of lightning are seen up to just above 200hPa. However, this is a limitation of the model, which has no stratospheric chemistry calculations, and therefore, the upper boundary of ozone affected by lightning NO_x could possibly be higher. Another small maximum between 8 and 12ppbv is seen over the southern United States. Comparing these with the lightning flashes seen in Figure 4, it can be seen that NO_x produced from lightning is transported into the tropical belt and the southern subtropics, contributing to the ozone maximum seen in Figure 7. The tropics are a chemically dynamic as well as physically dynamic area. The NO_x that is transported to and formed in the tropics, will add significantly to the ozone concentration there as well as affecting other regions through convection and transport.

The JJA maximum in the tropics is also seen in the DJF season, but extends farther

south from 10N to 45S, with an effect of lightning between 8 and 20ppbv. DJF is the Southern Hemisphere summer, and intuitively, the southerly shift in the maximum makes sense, however some ozone appears to be transported into the northern hemisphere. Comparing these figures to Figure 6, the correspondence of lightning occurrence and ozone transport is significant.

The plume of ozone found over South America extending over the South Atlantic and over South Africa is of great interest. This region is highly convective, and is also a region of biomass burning. The biomass-burning season runs from July to late September in the southern hemisphere tropical belt. In November and December, biomass burning is most intensive in Northern Africa, although significant burning takes place in South Africa as well. It is possible that this plume of ozone due to lightning NO_x is enhanced in this region due to biomass burning byproducts being transported to the upper troposphere by convection.

In an NCAR study using the MOZART model, a 10-20 ppbv increase in upper tropospheric ozone attributed to lightning was documented for approximately the same two seasons (Hauglustaine et al., 2001). The same upper tropospheric ozone plume extending over the western Pacific and eastern Indian Ocean was seen in their results from mid-November to December, which they attributed to lightning NO_x . The results presented here are also comparable to a study done with the Harvard Chemical Transport Model (Staudt et al, 2002).

Regional tracer experiment

The model includes six regional tracers, which tag chemically formed ozone in their respective region. The regions are as follows: Region 1, is lower tropospheric Northern Hemisphere (approximately 30N-90N); Region 2, lower tropospheric tropics (approximately 30N-30S); Region 3, lower

tropospheric Southern Hemisphere (approximately 30S-90S); Region 4, upper tropospheric Northern Hemisphere; Region 5, upper tropospheric tropics; and Region 6, upper tropospheric Southern Hemisphere.

Regional tracer experiments of the control run for JJA and DJF are shown in Figures 9 and 10. These figures show the percent of regional O_x tracer to the total O_x tracer. Comparing Figure 9 and 10 regions 1,3,4, and 6, we see major differences between hemispheres. In the summer season (JJA for N. Hemisphere and DJF for S. Hemisphere), there is more ozone chemically formed due to an increase in photolysis. One interesting point to make is that the Northern Hemisphere winter (Figure 10 regions 1,4) has more chemically produced ozone than the Southern Hemisphere summer (Figure 10 regions 3,6), which may be due to higher precursor emissions. Region 2 and 5, for both seasons, indicated stratospheric-tropospheric mixing. Approximately 40-70% of the chemically produced ozone in region 5 gets entrained in the circulation patterns above 150hPa for both JJA and DJF. The amount of chemically produced ozone in region 5 being transported downward and into other regions is small but significant. In JJA, 10-40% of total ozone tracer is transported to the Southern Hemisphere from upper troposphere to the surface. In DJF, 10-30% of the total ozone tracer is transported to the Northern Hemisphere down to just below 800hPa. In region 2, the tracer at the surface in the tropics shows for both seasons, vertical transport. In JJA, 10-20% of the total ozone tracer is transported to the southern subtropics up to about 400hPa, and up to the stratosphere just west of the equator. In DJF, 10-20% of the chemically produced ozone is transported up to the stratosphere and into the northern subtropics well above 500hPa.

These experiments demonstrate where ozone that is chemically produced in the tropics by lightning NO_x will possibly be

transported. Ozone chemically produced in the upper troposphere by lightning NO_x may be transported up to the stratosphere, and cycled back down in the midlatitudes due to Hadley cell circulation, or it may be transported down closer to the surface and depending on which season, either transported to the Northern or Southern Hemisphere.

Radiative Forcing

The global mean radiative forcing at the tropopause from tropospheric ozone produced from lightning NO_x for JJA (Figure 11a) is 0.12 Wm^{-2} . Maximum values occur in the southern subtropics and are as high as 0.32 Wm^{-2} . Radiative forcing for JJA is as small as -0.08 Wm^{-2} in the North Pole region, and in general, the tropics region is in the range of 0.08 to 0.16 Wm^{-2} . The global mean radiative forcing from tropospheric ozone produced by lightning NO_x is overall less in DJF (Figure 11b). The seasonal average is 0.1 Wm^{-2} , with a maximum occurring in the North pole region between 0.24 and 0.32 Wm^{-2} . The midlatitudes (around 45N) and southern subtropics ($\sim 25\text{S}$), during DJF, are affected by a 0.16 to 0.24 Wm^{-2} radiative forcing. Minimum radiative forcing occurs in the South Pole, and is as small as -0.08 Wm^{-2} . The bands of stronger radiative forcing seen in each plot are due to higher concentrations of ozone at the tropopause at these latitudes. These forcings are small compared to the radiative forcing of tropospheric ozone from pre-industrial to present day. The study from Shindell et al. (2003) documents a radiative forcing from the same model of 0.35 Wm^{-2} in JJA, and 0.26 Wm^{-2} in DJF. In a study by Toumi et al. (1996), a 0.1 Wm^{-2} global mean radiative forcing for tropospheric ozone was found for a 20% increase in lightning (from 5 Tg N yr^{-1} to 6 Tg N yr^{-1}). That increase is only a sixth of the increase in our study. There is a significant difference, which could be attributed to the simplicity of the model used in their study.

Doubled CO_2 experiment: Lightning and surface temperature

The relationship between the number of lightning flashes and surface temperature changes has been examined by Williams (1992), Toumi et al. (1996), Sinha and Toumi (1997), and Price and Rind (1994). They have documented that for a 20% increase in lightning the global mean radiative forcing by tropospheric ozone is about $+0.1 \text{ W m}^{-2}$. Price and Rind (1994), using the 9 layer GISS GCM with a different convection scheme, found a 10% total global increase, and up to a 30% local increase in lightning per degree of warming.

An experiment was done using the 23-layer GISS GCM with coupled chemistry in a doubled CO_2 climate simulation. Figure 13 shows the difference in the NO_x produced by lightning in the model between the doubled CO_2 experiment and the control for JJA and DJF. The majority of lightning NO_x is between 500 and 200 hPa, with a little at the surface between the equator and approximately 45N for JJA. In DJF, lightning NO_x produced in the model is from 500 to 150 hPa with some surface NO_x between the equator and 30S . Figure 14 shows the surface temperature change, in degrees Celsius, in response to the doubled CO_2 climate. There is approximately a 27% increase in lightning per degree of warming in JJA, and approximately a 22% increase in lightning per degree of warming in DJF. These figures were calculated by integrated total lightning over the globe for each simulation, taking the difference and dividing by the total integrated lightning for the control, then dividing by the average temperature increase.

CONCLUSION

Tropospheric ozone produced by lightning NO_x was examined using the NASA Goddard Institute for Space Studies global climate model with interactive chemistry. The model

predicts lightning produced tropospheric ozone concentrations comparable to other models, with seasonal global averages ranging from 4 to 6 ppbv in the upper troposphere. The tropical tropospheric ozone produced in the model by lightning is a large feature seen throughout the troposphere, and has been documented in other studies. Further study on this area could show that this plume of ozone in JJA and DJF could be attributed to mostly lightning and biomass burning byproducts. The model shows that the tropics are an extremely important area for ozone production by lightning, as well as an important area for the transport of ozone and its precursors to tropospheric ozone production. Tracers of chemically produced ozone show transport into the stratosphere from the upper troposphere, as well as a small percentage being transported between the tropics and each hemisphere.

The model results also show the radiative forcing of tropospheric ozone produced by lightning NO_x is small, but not negligible. Total radiative forcing for JJA and DJF is around 0.1Wm^{-2} , with outgoing longwave radiation making up most of the total, and shortwave contributing a very small number. Doubled CO_2 simulations show that lightning increases 20 to 30% per degree of warming in DJF and JJA, respectively. This implies the possibility of a positive feedback mechanism. Warming due to an increase in CO_2 causes an imbalance in the earth's radiation budget causing an increase in convection, which increases lightning. If lightning increases, this implies that NO_x will increase, increasing tropospheric ozone, which acts to further imbalance Earth's radiation budget. The possibility of a positive feedback mechanism in connection to lightning NO_x and tropospheric ozone is an important issue, which could be examined further using the GISS GCM with interactive chemistry. The addition of stratospheric chemistry calculations to the model is an important next step

to this study, as well as further examining the effect of lightning NO_x on ozone in the mid-to-high latitudes.

REFERENCES

- Benkovitz, C.M., M.T. Scholtz, J. Pacyna, L. Tarrason, J. Dignon, E.C. Voldner, P.A. Spiro, J.A. Logan, and T.E. Graedel. Global gridded inventories of anthropogenic emissions of sulfur and nitrogen. *J. Geophys. Res.* 101, 29,239-29,253, 1996.
- Chameides, W.L., and J.C.G. Walker. A photochemical theory of tropospheric ozone, *J. Geophys. Res.*, 78, 8751-8760, 1973.
- Crutzen P.J., A discussion of the chemistry of some minor constituents in the stratosphere and troposphere, *Pure Appl. Geophys.*, 106-108 1385, 1973.
- Crutzen P.J. Photochemical reaction initiated by and influencing ozone in unpolluted tropospheric air, *Tellus*, 26, 45-55, 1974.
- Exhalt, D.H. Gas phase chemistry of the troposphere. Chapter 2 in *Global Aspects of Atmospheric Chemistry*, edited by Deutsche Bunsen-Gesellschaft für Physikalische Chemie e.V., R. Zellner guest editor, Darmstadt Steinkopff, New York, Springer, pp. 21-109, 1999.
- Fung, I., J. John, J. Lerner, E. Matthews, M. Prather, L.P. Steele, and P.J. Fraser. Three-dimensional model synthesis of the global methane cycle. *J. Geophys. Res.*, 96, 13,033-13,065, 1991.
- Gery, M.W., G.Z. Whitten, J.P. Killus, M.C. Dodge. A photochemical kinetics mechanism for urban and regional scale computer modeling. *J. Geophys. Res.*, 94, 925-956, 1989.

- Grewe, V., D. Brunner, M. Dameris, J.L. Grenfell, R. Hein, D. Shindell, J. Staehelin. Origin and variability of upper tropospheric nitrogen oxides and ozone at northern mid-latitudes. *Atmos. Env.*, 35, 3421-3433, 2001.
- Haagen-Smit, A.J., Darley, E.F., Zaitlin, M., Hull, H. and Noble, W. Investigation on injury to plants from air pollution in the Los Angeles area. *Plant Physiology*, 27, 18–34, 1952.
- Hansen, J., et al. A Pinatubo climate investigation, in *The Effects of Mt. Pinatubo Eruption on the Atmosphere and Climate*, NATO ASI Ser. Subser. 1, Global Environmental Change, edited by G. Fiocco, D. Fua, and G. Visconti, pp. 233-272, Springer-Verlag, New York, 1996.
- Hauglustaine, D., L. Emmons, M. Newchurch, G. Brasseur, T. Takao, K. Matsubara, J. Johnson, B. Ridley, J. Stith, and J. Dye. On the Role of Lightning NO_x in the Formation of Tropospheric Ozone Plumes: A global Model Perspective. *J. Atmos. Chem.* 38, 277-294, 2001.
- Holland E.A., F.J. Dentener, B.H. Braswell and J.M. Sulzman. Contemporary and pre-industrial reactive nitrogen budgets. *Biogeochemistry*, 46, 7-43, 1999.
- Houweling, S., T.L. Schneider, R.W. Protmann, S. Solomon. Climate forcing due to tropospheric and stratospheric ozone. *J. Geophys. Res.*, 103, 10,673-10,696, 1998.
- Intergovernmental Panel on Climate Change, Climate Change 2001. J.T. Houghton, et al (eds). Cambridge University Press, Cambridge England, 881 pp., 2001.
- Lee, D.S., I. Kohler, E. Grobler, F. Rohrer, R. Sauen, L. Gallardo-Klenner, J.J.G. Olivier, F.J. Dentener and A.F. Bouwman. Estimates of global NO_x emissions and their uncertainties. *Atmos. Env.*, 31, 1735-1749, 1997.
- Levy, H.I. Normal Atmosphere: Large Radical and Formaldehyde Concentrations Predicted. *Science*, 173, 141, 1971.
- Olivier, J.G.J., A.F. Bouwman, C.W.M. Vander Maas, J.J.M. Berdowski, C. Veldt, J.P.J. Bloos, A.J.H. Visschedijk, P.Y.J. Zandveld, J.L. Haverlag. Description of EDGAR Version 2.0: A set of global emission inventories of greenhouse gases and ozone-depleting substances for all anthropogenic and most natural sources on a per country basis and on 1x1 grid. RIVM Techn. Report nr. 771060 002; TNO-MEP report nr. R96/119. National Institute of Public Health and the Environment, Bilthoven, December 1996.
- Penner, J.E., Lister, D.H., Griggs, D.J., Dopkken, D.J.&McFarland, M., eds. (1999) *Aviation and the Global Atmosphere: A Special Report of IPCC Working Groups I and III* (Cambridge Univ. Press, New York).
- Pickering, K.E., Y. Wang, W. Tao, C. Price, and J.F. Muller. Vertical distributions of lightning NO_x for use in regional and global chemical transport models. *J. Geophys. Res.*, 103, 31,203-31,216, 1998.
- Prather, M. Numerical advection by conservation of second-order moments. *J. Geophys. Res.*, 91, 6671-6681, 1986.
- Price, C., and D. Rind. Possible implications of global climate change on global lightning distributions and frequencies. *J. Geophys. Res.*, 99, 10,823-10,831, 1994.
- Price, C., J. Penner, and M. Prather. NO_x from lightning 1. Global distribution based on

- lightning physics. *J. Geophys. Res.*, 102, 5929-5941, 1997.
- Shindell, D.T., J.L. Grenfell, D. Rind, and V. Grewe. Chemistry-climate interactions in the Goddard Institute for Space Studies general circulation model 1. Tropospheric chemistry model description and evaluation. *J. Geophys. Res.*, 106, 8047-8075, 2001.
- Shindell, D.T., G. Faluvegi, and N. Bell. Preindustrial-to-present-day radiative forcing by tropospheric ozone from improved simulations with the GISS chemistry climate GCM. Submitted 2003.
- Sinha, A. and R. Toumi. Tropospheric ozone, lightning, and climate change. *J. Geophys. Res.*, 102, 10,667-10,672, 1997.
- Staudt, A. C., D. J. Jacob, J. A. Logan, D. Bachiochi, T. N. Krishnamurti, and N. I. Poisson, Global chemical model analysis of biomass burning and lightning influences over the South Pacific in austral spring. *J. Geophys. Res.*, 2002.
- Tie, X., R. Zhang, Guy Brasseur, and W. Lei. Global NO_x Production by Lightning. *J. Atmos. Chem.*, 43, 61-74, 2002.
- Toumi, R., J.D. Haigh, and K.S. Law. A tropospheric ozone-lightning climate feedback. *Geophys. Lett.*, 23, 1037-1040, 1996.
- Wang, Y., D. Jacob, J. Logan. Global simulation of tropospheric O₃-NO_x hydrocarbon chemistry, 1, Model formulation. *J. Geophys. Res.*, 103, 10,713-10,725, 1998.
- Wild O., X. Zhu, M.J. Prather. Fast-J: Accurate simulation of in-and-below-cloud photolysis in tropospheric chemical models. *J. Atmos. Chem.*, 37, 245-282, 2000.
- Williams, E.R. The Schumann resonance-A global tropical thermometer. *Science*. 256, 1184-1187, 1992.
- Zel'dovich, Y.B. and Y.P. Raizer, *Physics of Shock Waves and High-Temperature Hydrodynamic Phenomena*, 445pp., Academic, San Diego, Calif., 1966.

LIST OF FIGURES

Figure 1a-b. Seasonal averages of total model ozone (Dobson Units) for a) June, July and August, and b) December, January, and February.

Figure 2a-b. Zonally averaged vertical distribution of O_x (10^{-8} ppv) for a) June, July, and August, and b) December, January, and February.

Figure 3a-b. Zonally averaged vertical distribution of NO_x (10^{-11} ppv) for a) June, July, and August, and b) December, January, and February.

Figure 4a-b. NO_x mixing ratio (10^{-11} ppv) difference between control run and no lightning run for a) June, July and August, and b) December, January, and February. Note that NO_x concentration includes sources and sinks.

Figure 5a-b. NO_x produced by lightning (10^{-2} kg/s) for a) June, July, and August, and b) December, January, and February. Note that this figure is only depicting NO_x from the lightning source calculated in the GISS model. No other sources or sinks are included here.

Figure 6. Total lightning flashes/time as calculated by the model. Top panel is lightning for June, July, and August, and the bottom panel is lightning for December, January, and February. Lightning flashes have highest occurrence during summer (JJA for Northern Hemisphere; DJF for Southern Hemisphere).

Figure 7a-f. (two pages) Ozone (ppbv) differences (control-no lightning case) averaged for June, July, and August at a) 171hPa, b) 218hPa, c) 279hPa, d) 370hPa, e) 498hPa, and f) 640hPa. The global mean is in the upper right corner of each plot.

Figure 8a-f. (two pages) Ozone (ppbv) differences (control-no lightning case)

averaged for December, January, and February at a) 171hPa, b) 218hPa, c) 279hPa, d) 370hPa, e) 498hPa, and f) 640hPa. The global mean is in the upper right corner of each plot.

Figure 9. June, July, and August percent of ozone regional tracer for regions 1,2,3 (top row, left to right), and regions 4,5,6 (bottom row, left to right). Regions 1,2, and 3 are lower tropospheric regional tracers while regions 4,5, and 6 are upper tropospheric tracers.

Figure 10. December, January, and February percent of ozone regional tracer for regions 1,2,3 (top row, left to right), and regions 4,5,6 (bottom row, left to right). Regions 1,2, and 3 are lower tropospheric regional tracers while regions 4,5, and 6 are upper tropospheric tracers.

Figure 11. Both panels show the total global radiative forcing (W/m^2) at the tropopause for tropospheric ozone. Plotted results are the difference between the control and no lightning experiment. The top panel is for June, July, and August, and the bottom panel is for December, January, and February.

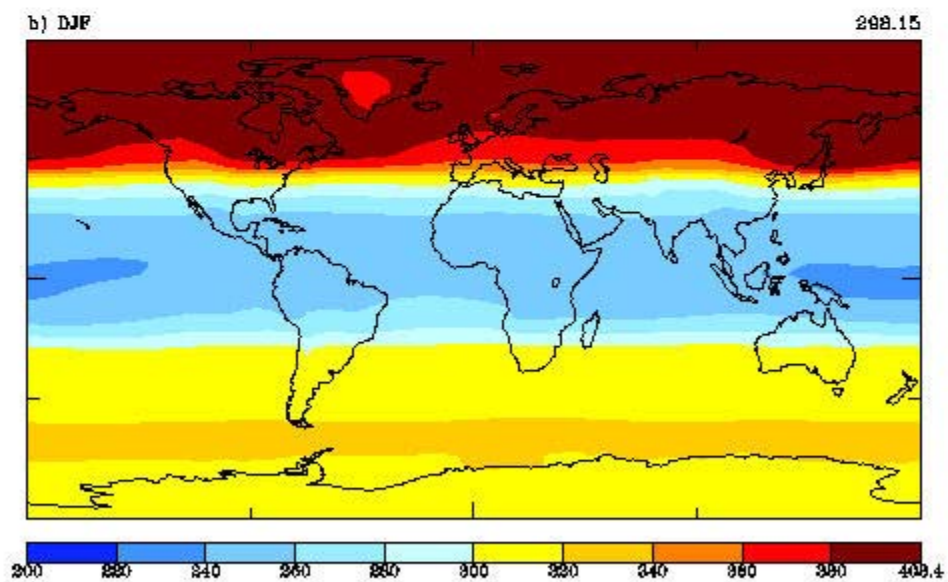
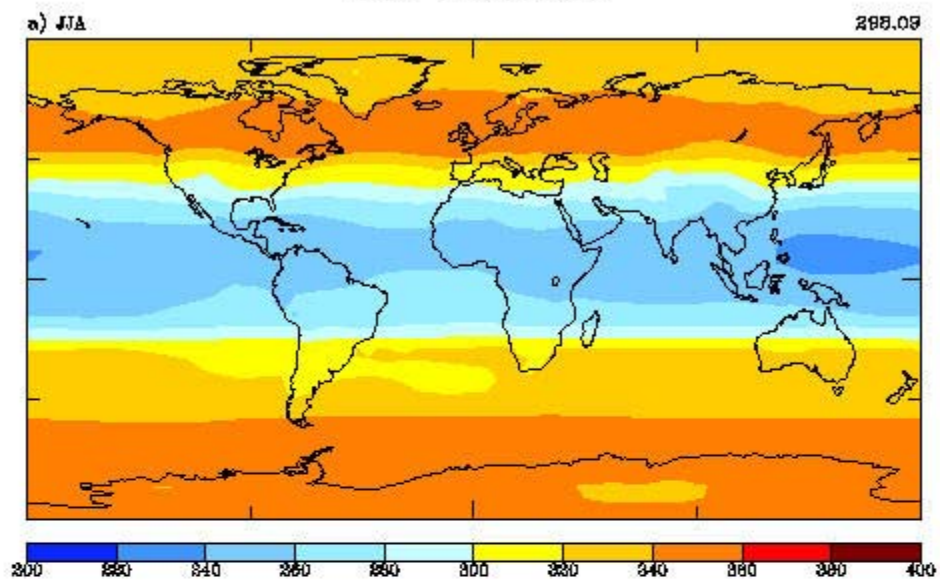
Figure 12. The downward shortwave radiative forcing is shown in the upper and lower left panels, and the downward longwave radiative forcing ($*-1$) is shown in the upper and lower right panels. Plotted results are the difference between the control and no lightning experiment. The top row is for June, July, and August, and the bottom row is for December, January, and February.

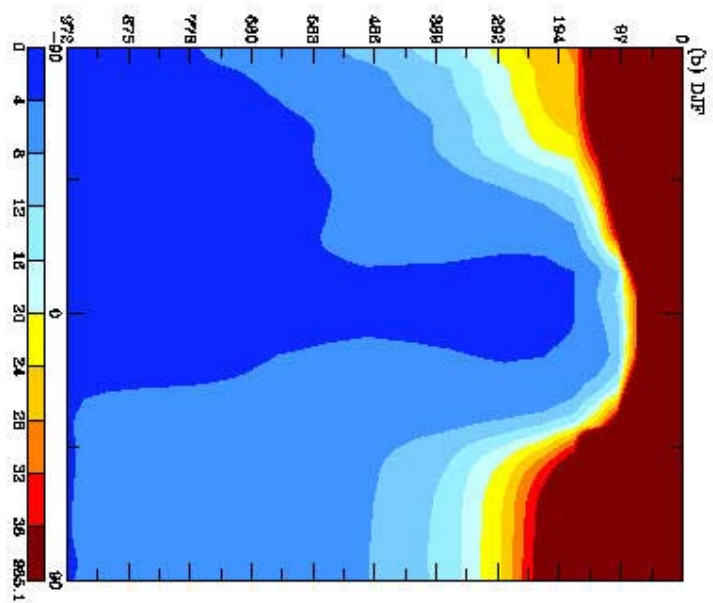
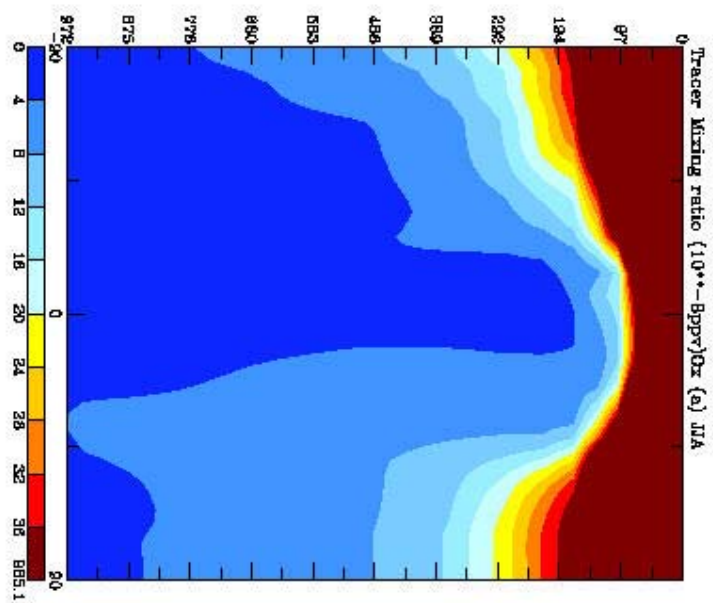
Figure 13a-b. Lightning produced NO_x (10^{-2} kg/s) from the double CO_2 experiment. Plotted results show the difference between the double CO_2 run and the control for a) June, July, and August, and b) December, January, and February.

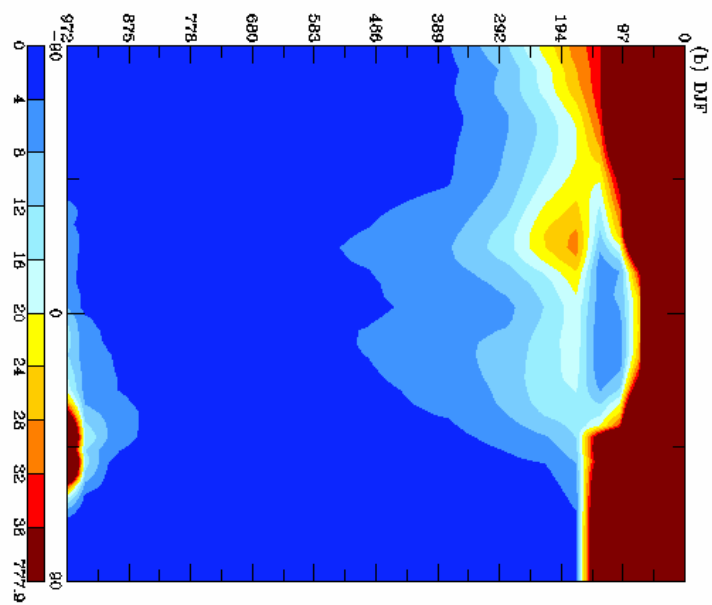
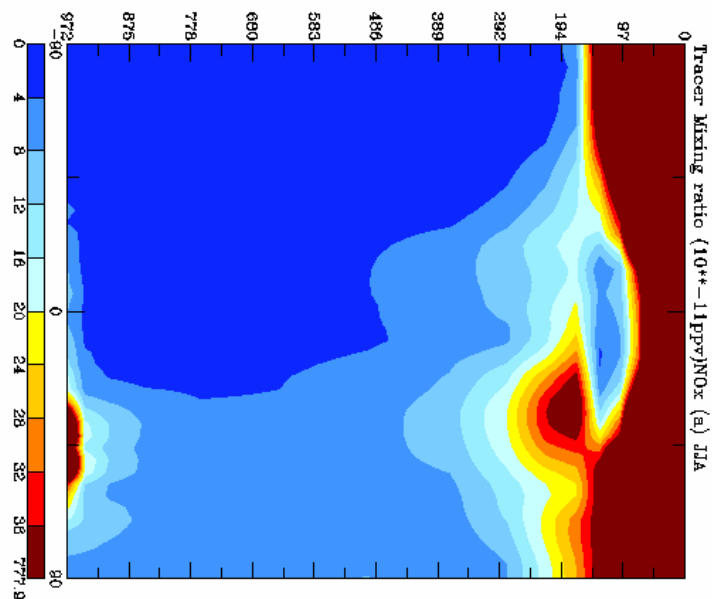
Figure 14a-b. Global surface temperature changes (Doubled CO_2 - control experiment) for a) June, July, and August, and b)

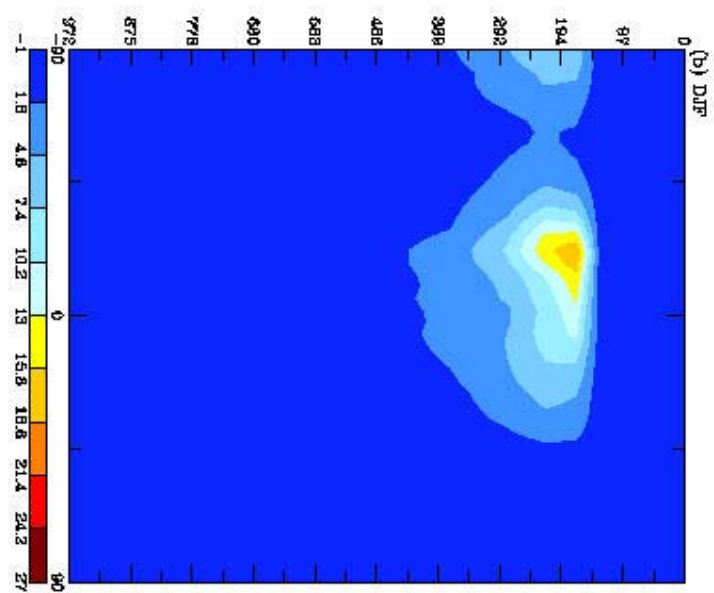
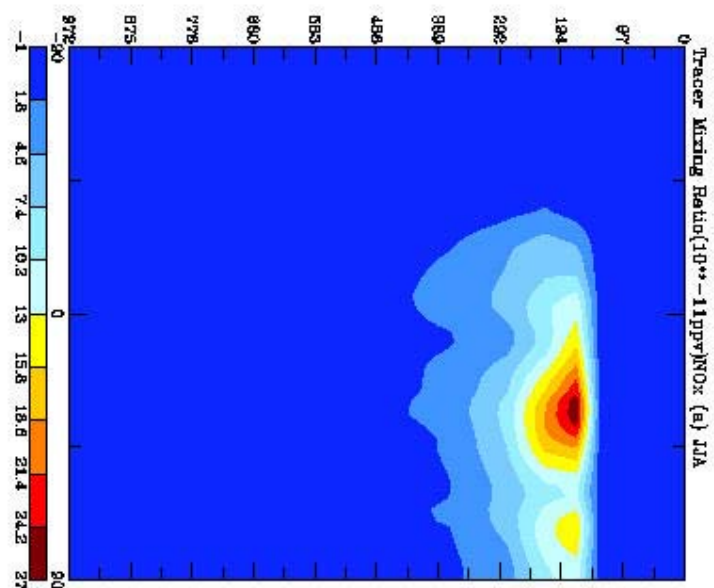
December, January, and February. Global averages are in the top righthand corner.

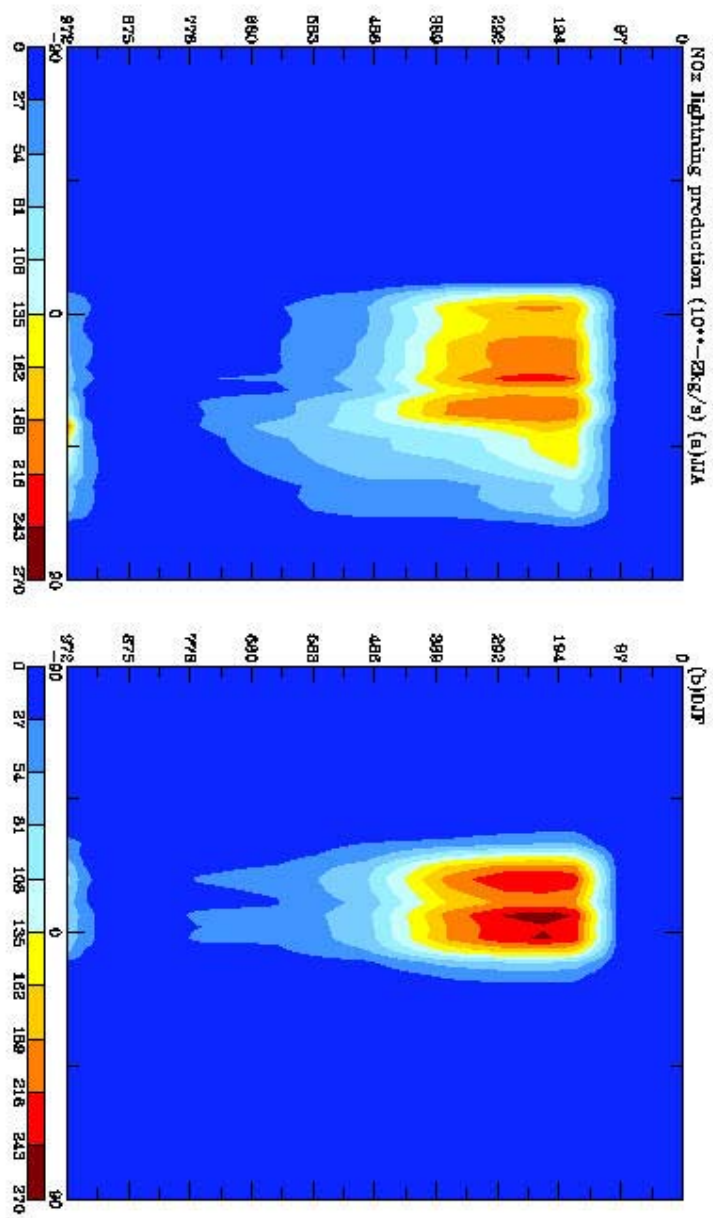
Total Ozone (DU)

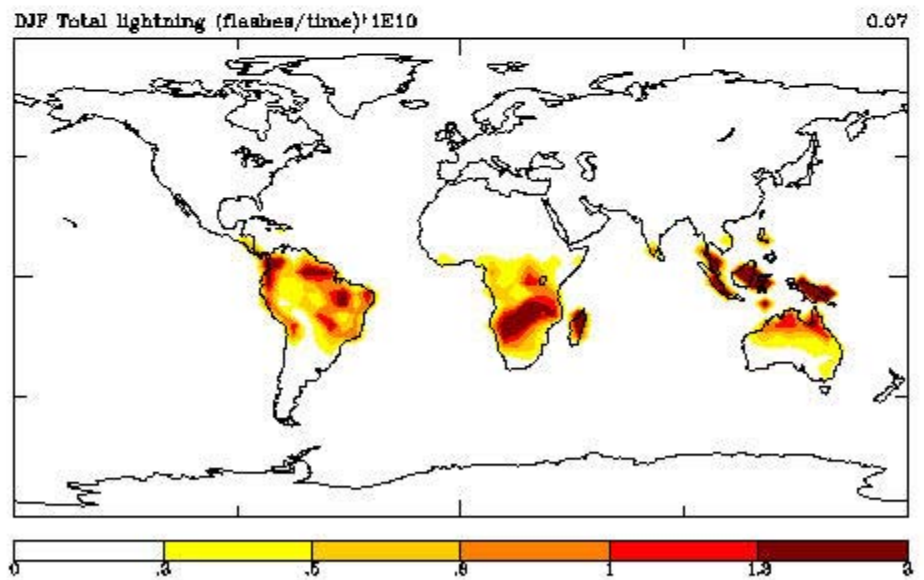
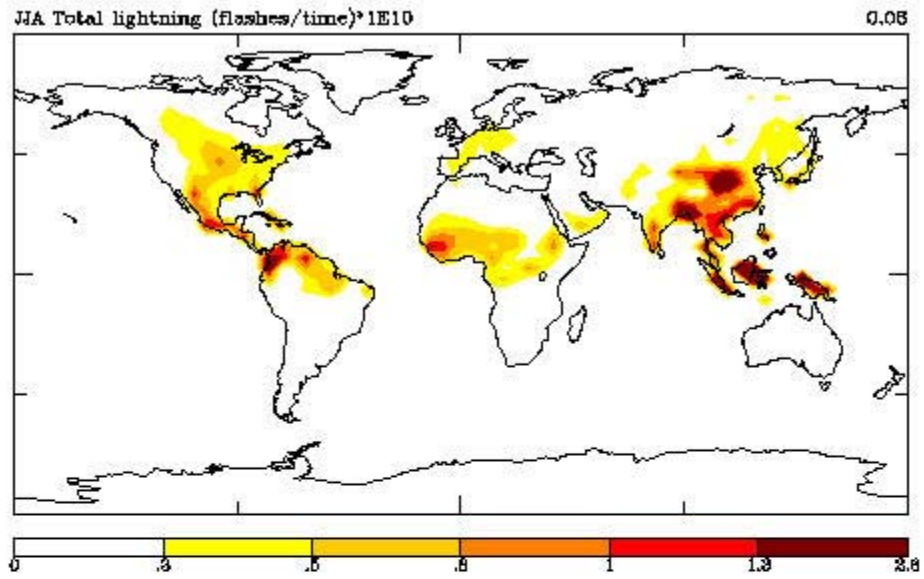


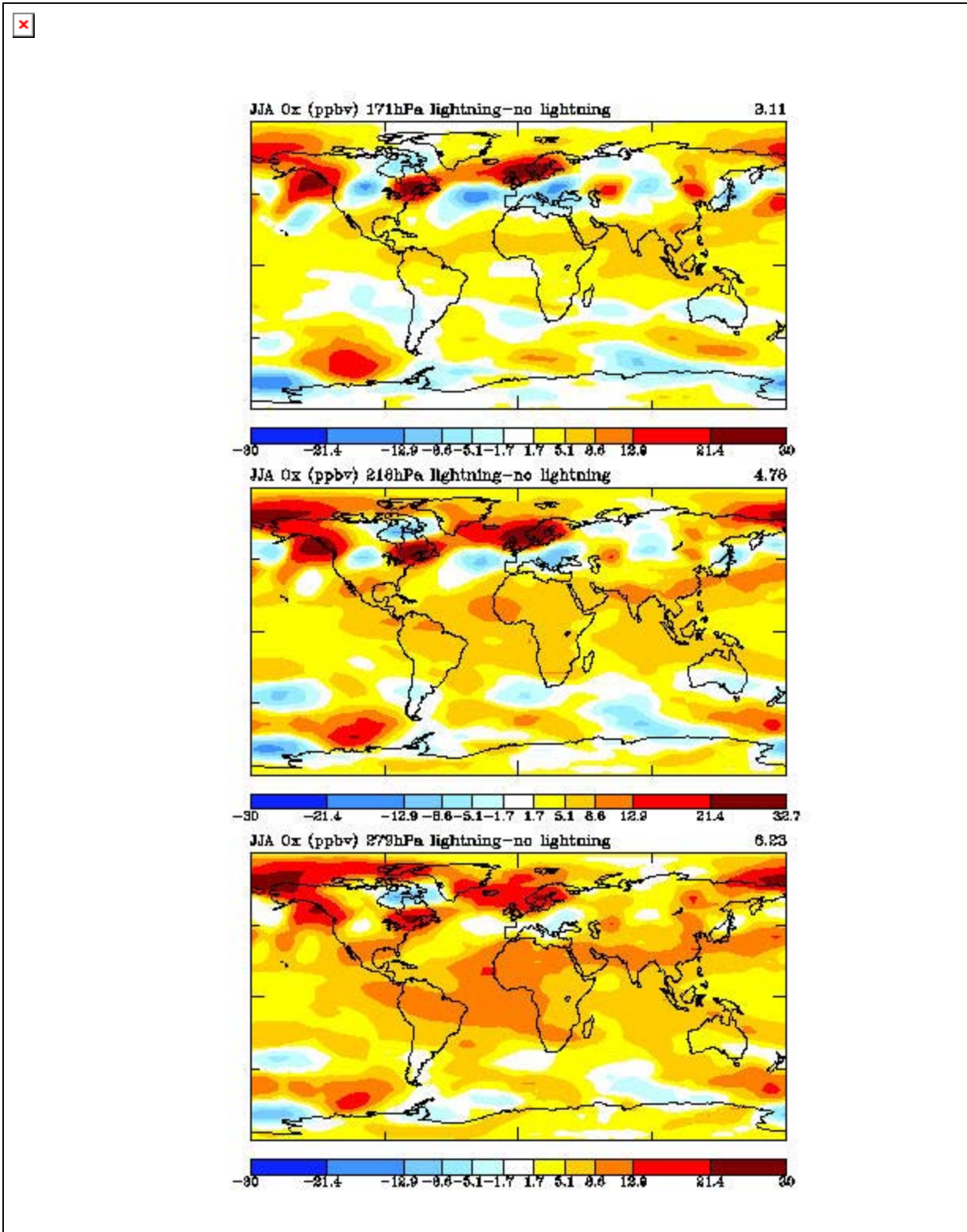


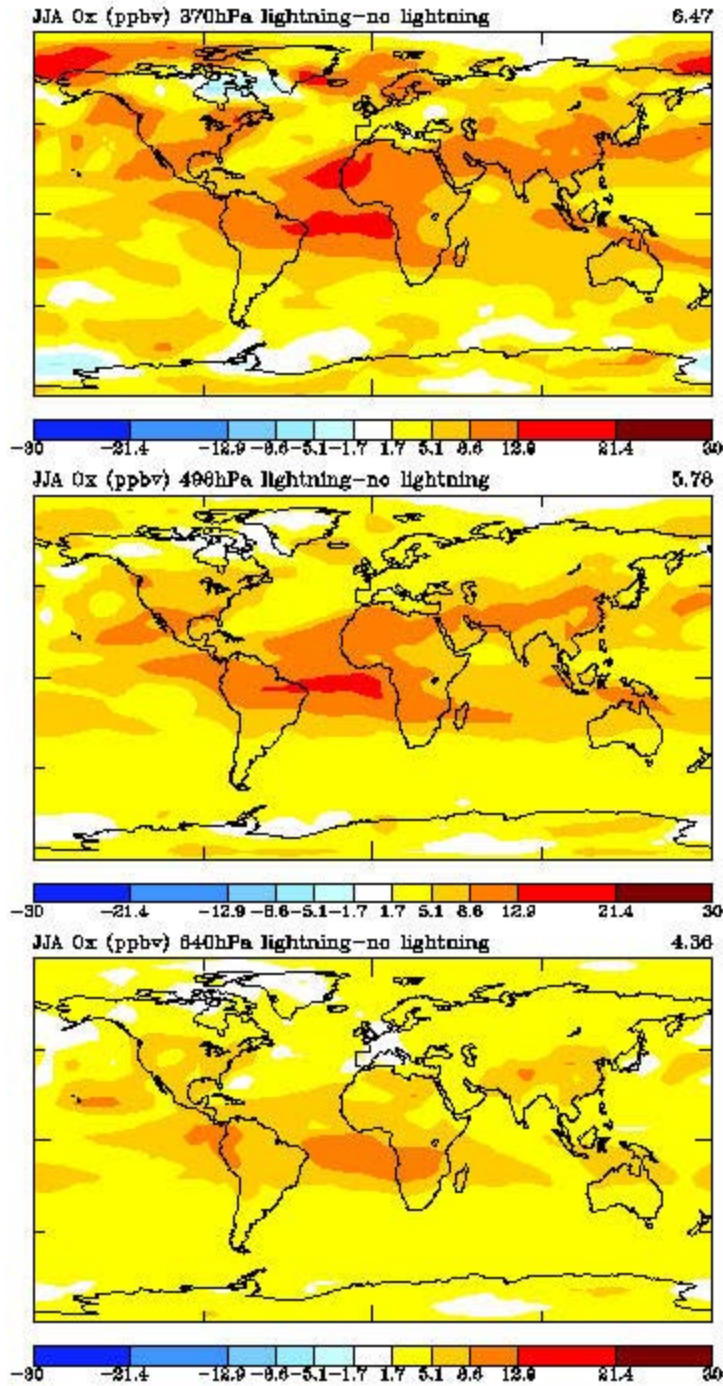


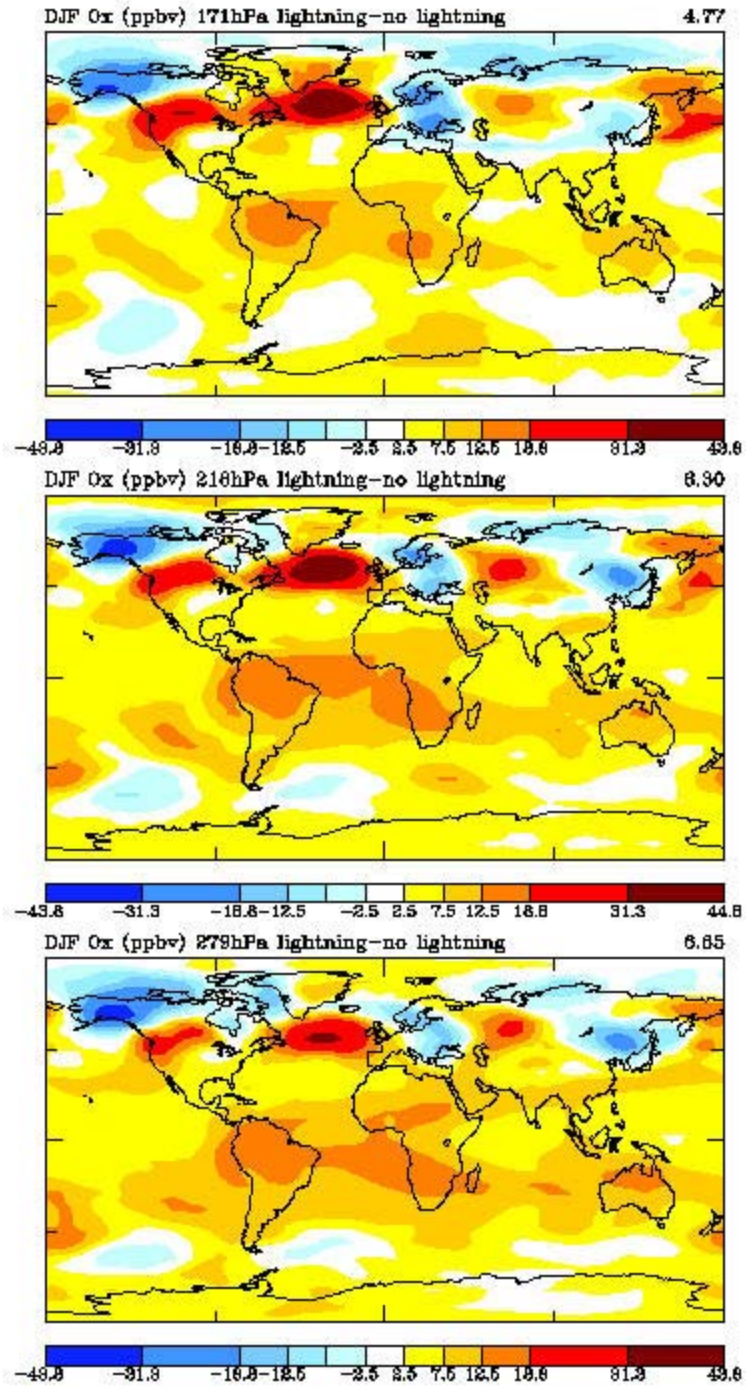


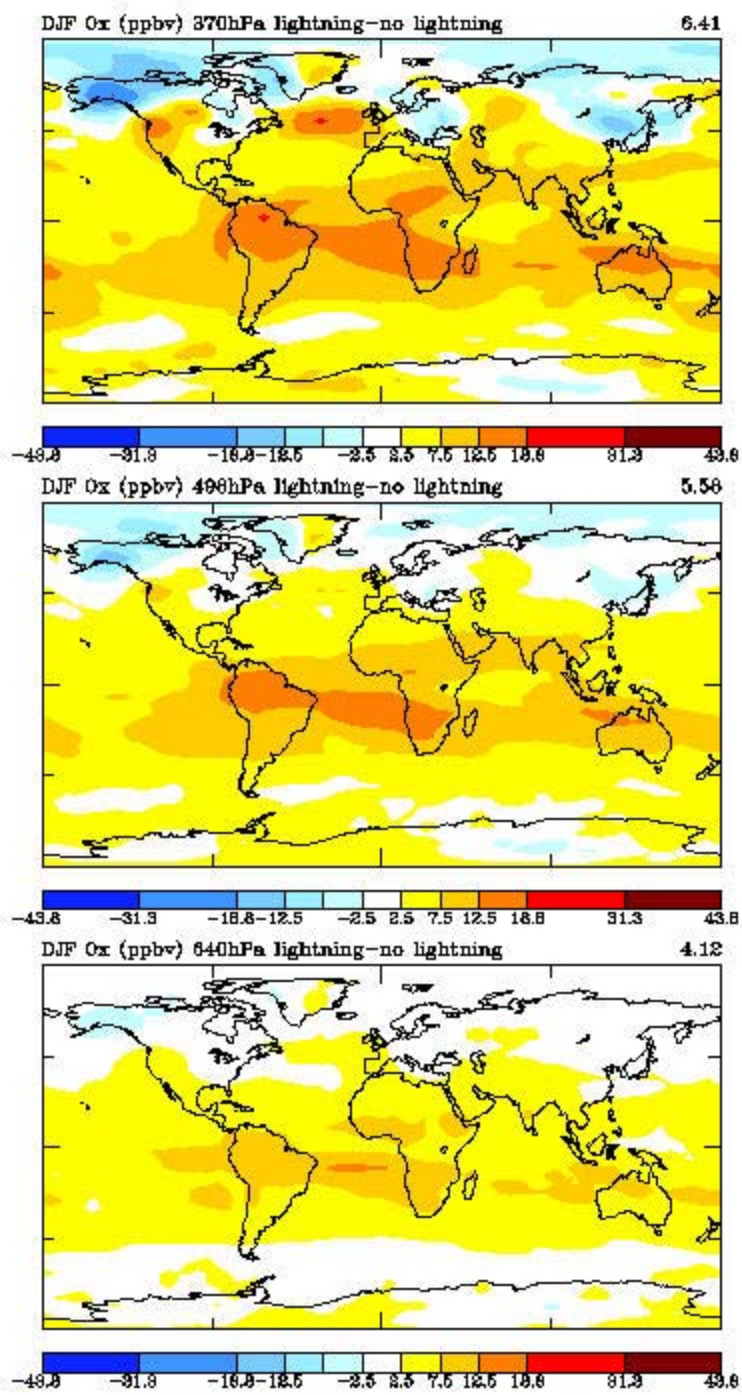


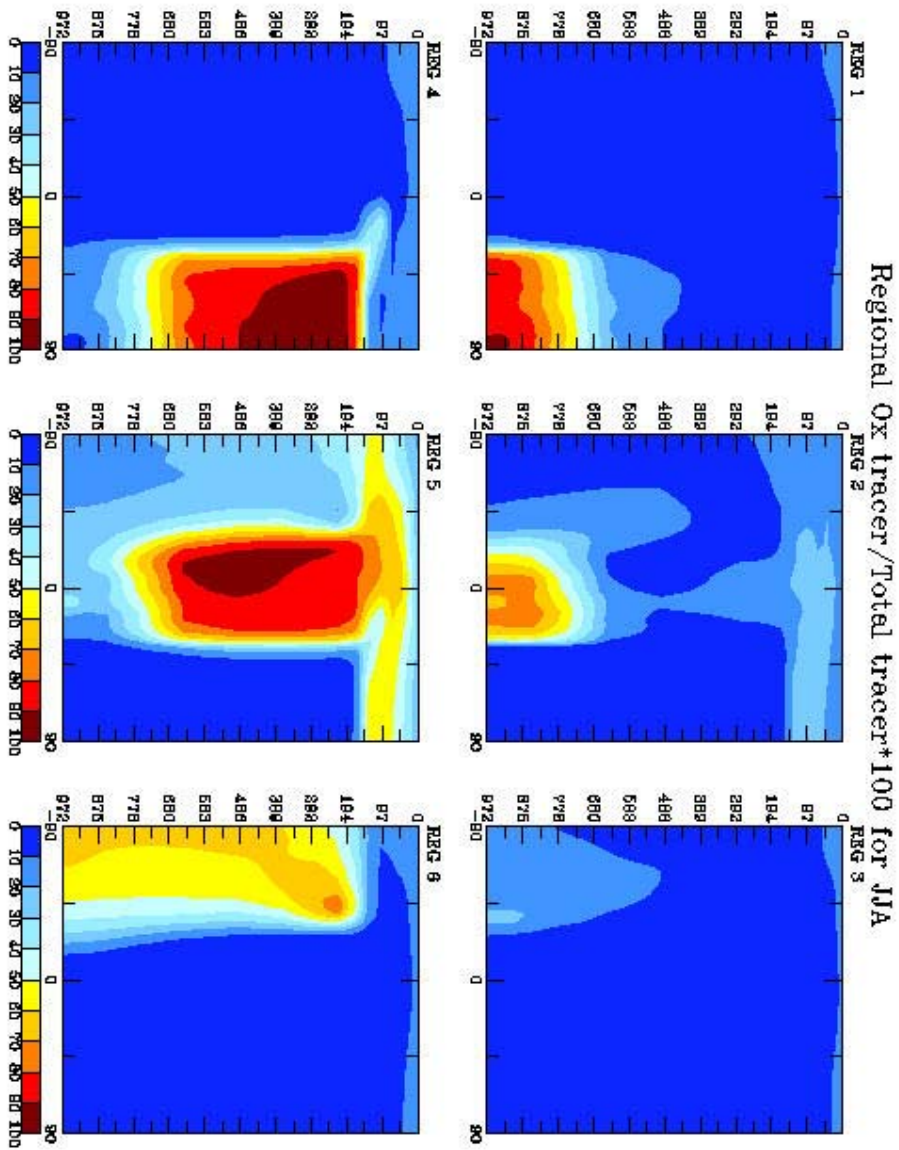


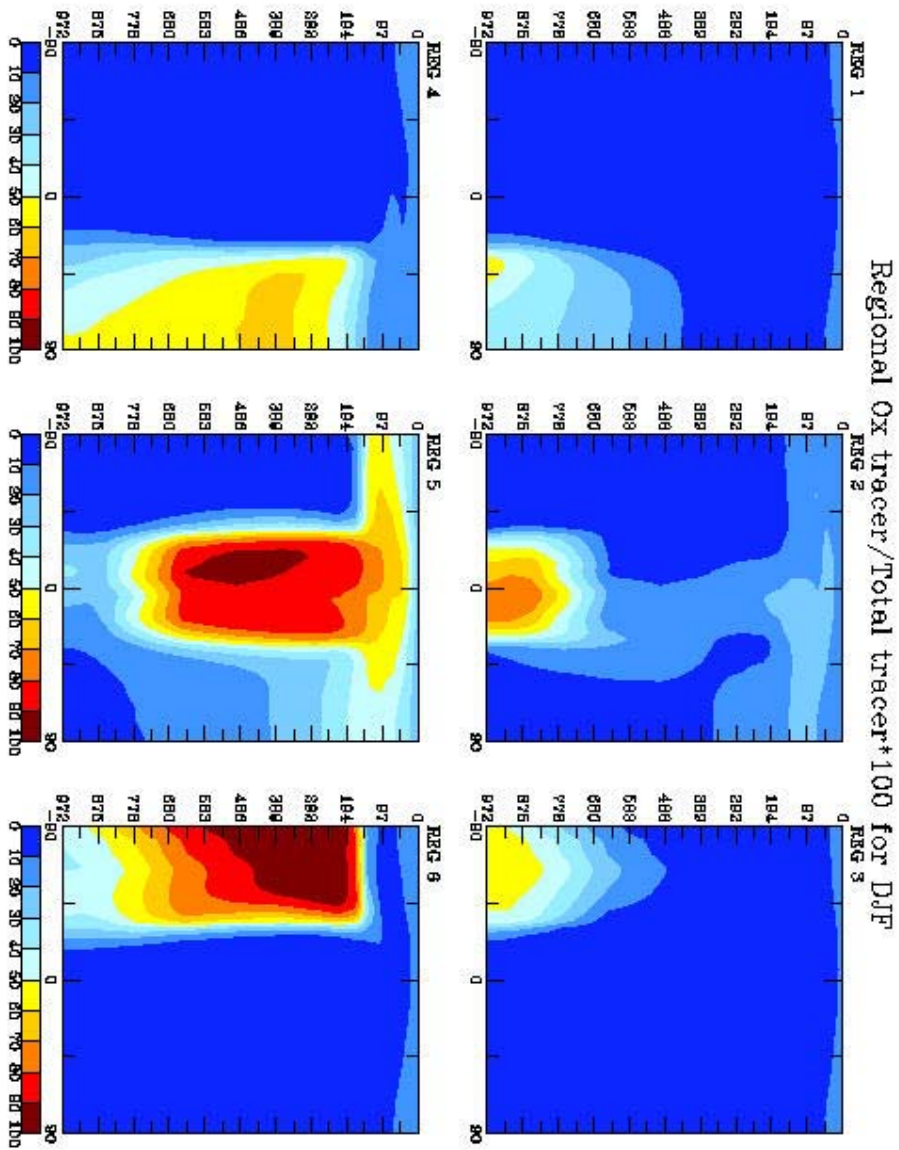


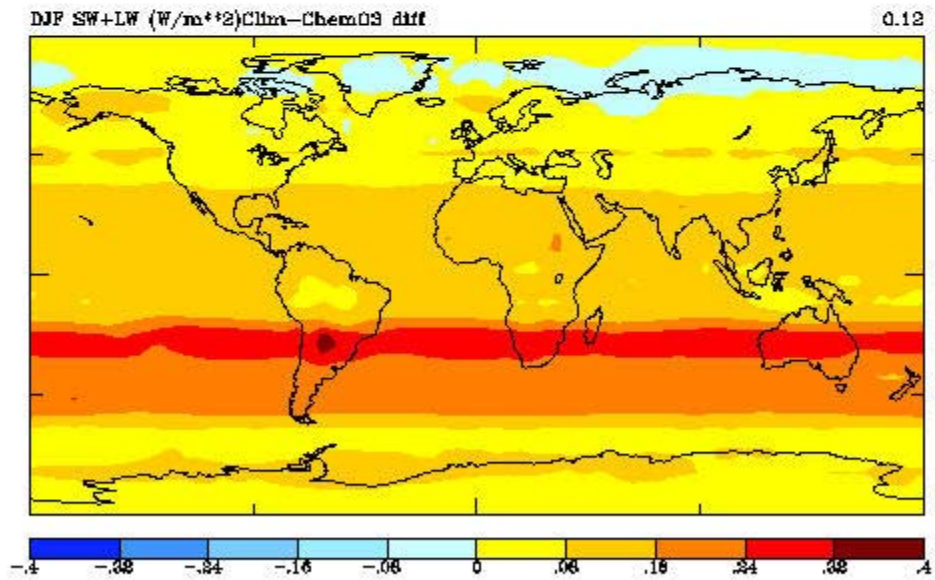
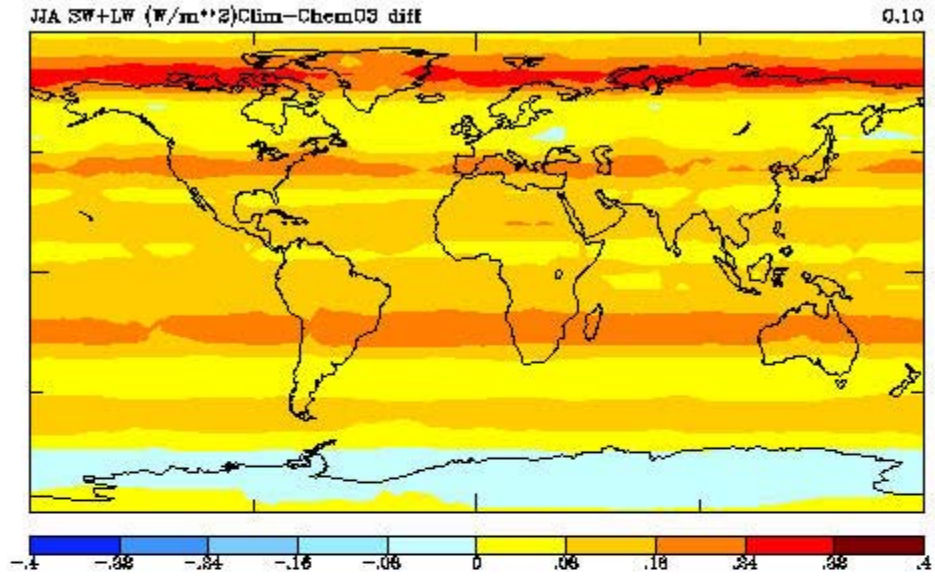


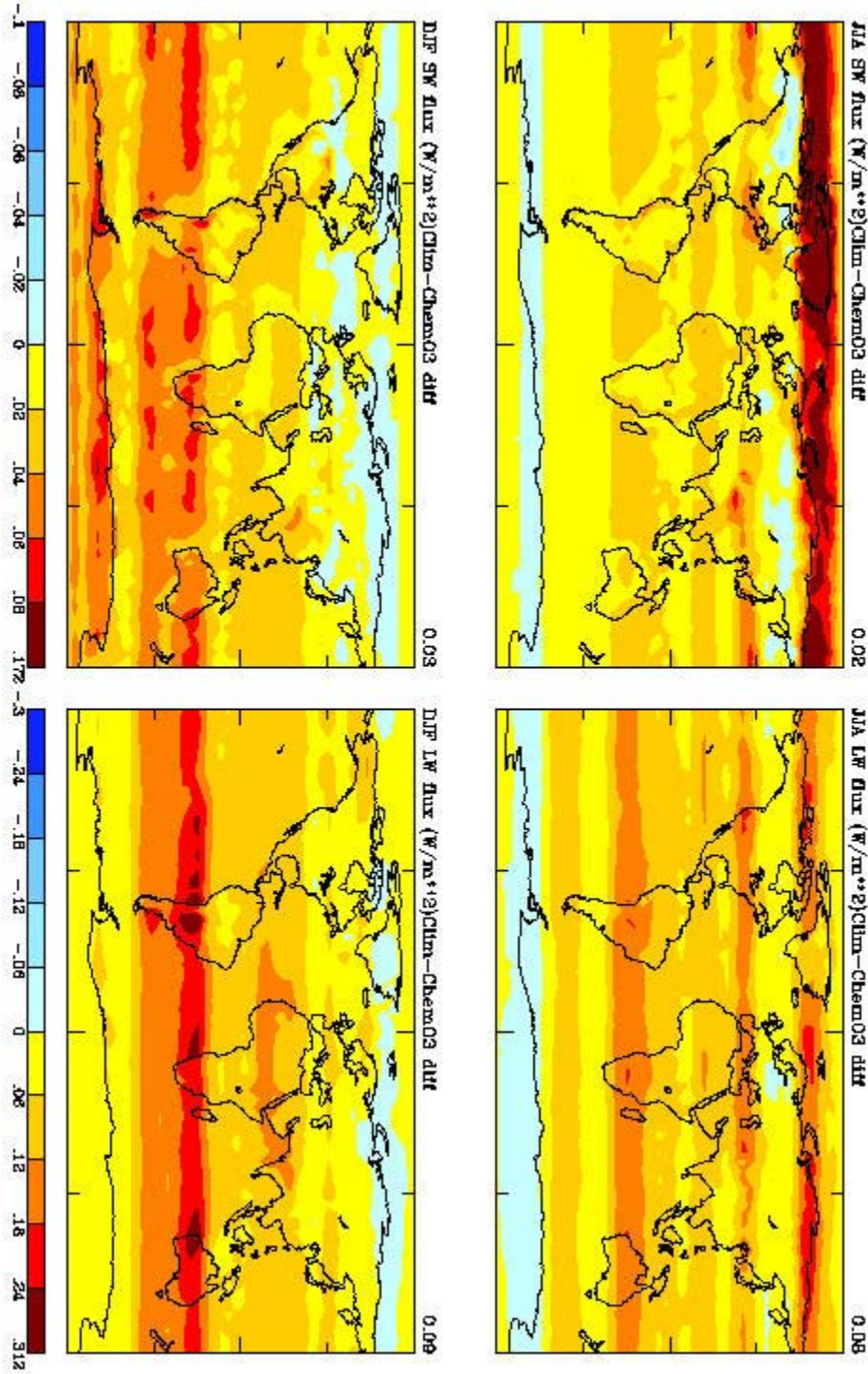


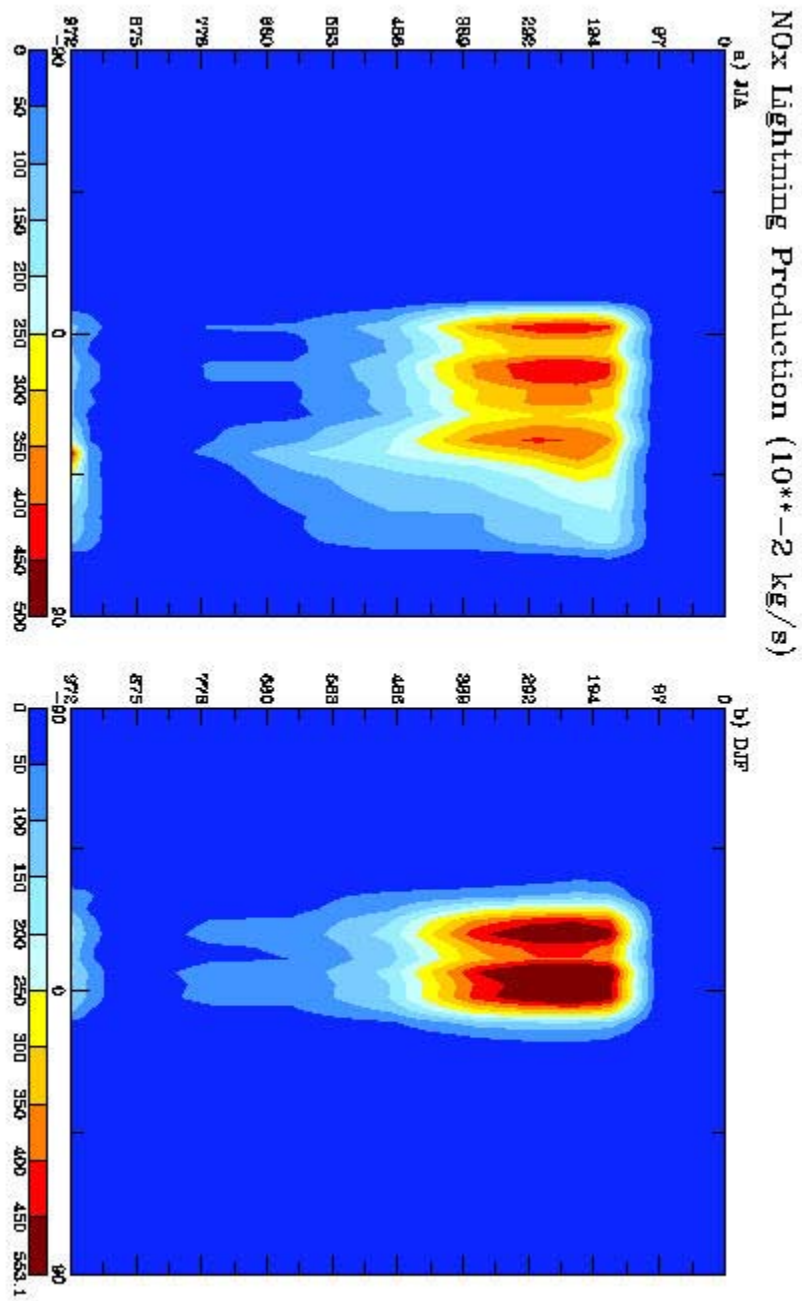








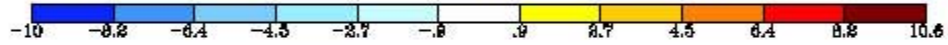
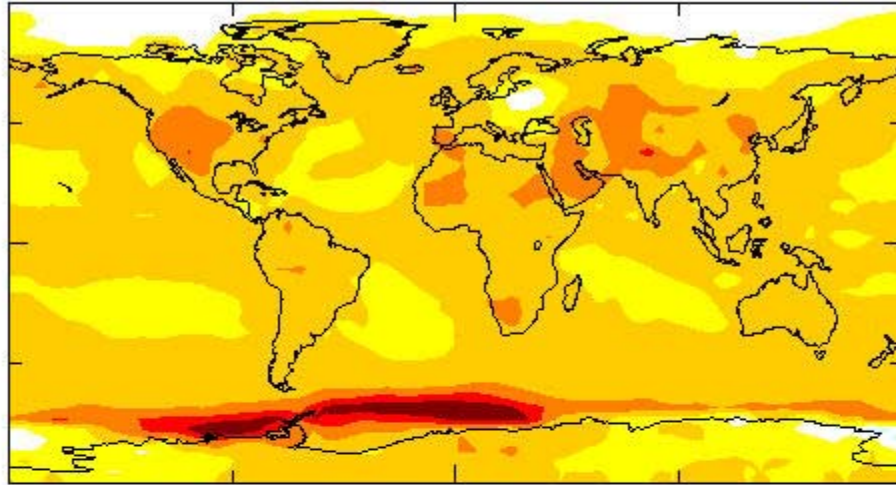




Surface Temperature (degrees C) DoubleCO2-control

a) JJA

5.29



b) DJF

3.83

